

Article

Experimental Study on Downhole Acoustic Wave Propagation Characteristics in Curved Drill String

Qing Wang ^{1,*}, Chenguang Bi ², Jiawei Zhang ¹, Haige Wang ¹ and Zhichuan Guan ³¹ CNPC Engineering Technology Research & Development Company Limited, Beijing 102206, China² CNPC Daqing Drilling & Exploration Engineering Company, Daqing 163458, China³ School of Petroleum Engineering, China University of Petroleum (East China), Qingdao 266580, China

* Correspondence: wq4967079@163.com

Abstract: Aiming at the problem of the unclear sound wave attenuation in the signal transmission of the load-bearing drill string, an experimental device for the sound wave propagation characteristics in the curved drill string was set up. The influence of the drill string structure and acoustic excitation parameters on the sound propagation characteristics in the drill string under different loads is different. The results show that the curvature of the drill string has an influence on the propagation of the sound wave in the drill string, and its rule is related to the curvature of the drill string and the frequency of the sound wave. The pulse repetition rate, excitation voltage, and pulse width only affect the passband amplitude, and the effect is significantly greater than the curvature of the drill string. The main influencing factor of its sound transmission characteristics is the degree of drill string curvature. The low-frequency signal should be preferentially selected as the carrier of downhole information transmission after considering the influence of drill string bending on acoustic transmission.

Keywords: curved drill string; acoustic propagation; spectrum; pulse; amplitude



Citation: Wang, Q.; Bi, C.; Zhang, J.; Wang, H.; Guan, Z. Experimental Study on Downhole Acoustic Wave Propagation Characteristics in Curved Drill String. *Processes* **2023**, *11*, 1525. <https://doi.org/10.3390/pr11051525>

Academic Editor: Sara Liparoti

Received: 1 December 2022

Revised: 7 February 2023

Accepted: 21 February 2023

Published: 17 May 2023



Copyright: © 2023 by the authors. Licensee MDPI, Basel, Switzerland. This article is an open access article distributed under the terms and conditions of the Creative Commons Attribution (CC BY) license (<https://creativecommons.org/licenses/by/4.0/>).

1. Introduction

The accurate and high-speed transmission of downhole information is one of the keys to retaining it safe and efficient with the coexistence of a multi-risk in complex drilling conditions. At present, conventional oil and gas resources have entered a stage of natural decline, and it is difficult to increase recovery. Unconventional oil and gas resources are a significant growth point for production with horizontal wells such as shale oil and gas. However, the downhole conditions are complicated and accidents occur frequently during the drilling of horizontal wells; the real-time and accurate grasp of the downhole conditions are the basis for reducing downhole accidents. The rapid development and wide application of intelligent measurement equipment meet the needs of downhole information collection, but it is difficult to transmit large-scale data to the ground with a high speed through the traditional mud pulse transmission method, which has become the main bottleneck restricting the safe and efficient drilling of horizontal wells [1]. The main method to solve the above problem is to develop a downhole information transmission system with a high speed, high accuracy, and strong anti-interference ability of the external factors.

The steel drill string is used as the transmission channel for the acoustic transmission of downhole information. Because the transmission process does not depend on drilling fluid and unlimited formation, it is expected to become a technological breakthrough [2] due to its advantages of simple equipment structure and easy directional transmission. Some acoustic transmission systems have been preliminary applied in the field, including the system and the wireless measurement-while-drilling (MWD) system developed by Halliburton and Baker Hughes. The maximum transmission depth and rate are 3600 m and 33 bps, showing a good application prospect [3–5]. These are also signs of staged

progress. The vibration wave communication technology has been tested in the information transmission of layered water injection [6], sand production information, and cluster well anti-collision [7]. Researchers have also studied the influence of different factors on the acoustic transmission characteristics in the drill string, including the combination method of the string [8], size characteristics [9–11], fluid damping [12], formation damping [13], noise [14,15], and transducer excitation parameters [16]. Additionally, basic transmission models and experimental devices [17–19] were set up due to the need for information transformation.

However, the downhole information acoustic transmission technology has not yet become the main measurement and control method in the field. The unclear transmission characteristics of acoustic waves in a drill string under different stress states is one of the difficulties that restricts the technology from theoretical research to field application [20–24]. When the acoustic wave propagates in the periodic string, it presents the characteristic of a comb filter in which the passband with less attenuation and the stopband with greater attenuation alternate due to the existence of the drill string coupling. The acoustic wave propagation characteristic is the theoretical basis of the frequency selection and the installation method of the repeater, it determines the transmission distance and accuracy of the acoustic signal in the drill string [25,26]. The inclination angle gradually increases from 0° to nearly 90° in the drilling process of a horizontal well, the drill string is in a curved state, and its acoustic wave propagation characteristics in the curved drill string become the key to acoustic signal transmission from the bottom hole to the ground smoothly.

In order to overcome the above problem, an acoustic emission device was developed and an experimental device for the acoustic propagation characteristics in the curved drill string was set up based on the bending state of the drill string under actual drilling conditions, and the influence of the bending state on the acoustic propagation in the drill string was carried out [27,28]. This research can be used for the application of the time carrier frequency selection and the establishment of the repeater installation method in the acoustic wave transmission technology of horizontal wells. It provides a theoretical basis for the comprehensive monitoring of the wellbore information of intelligent drilling and judging downhole risks to avoid drilling accidents.

2. Materials and Methods

2.1. Structural Design of Acoustic Emission/Reception Device

2.1.1. Selection of Downhole Signal Generator

The signal generator is mainly used to adjust the parameters such as the waveform, frequency, voltage, pulse width, pulse repetition rate, and duty cycle of the generated sound wave. The signal generator used in the experiment is the AFG3102 series arbitrary waveform generator of Tektronix Company (Figure 1). It can output arbitrary waveforms, the sampling rate of the memory: 16 K–128 K: 250 MS/s, 2 points-16 K: 1 GS/s, and has a 14-bit vertical resolution. The output bandwidth of the sine wave is 1 MHz–100 MHz; the output bandwidth of square wave is 1 MHz–50 MHz; the rise/fall time is ≤ 5 ns; the output bandwidth of the pulse waveform is 1 MHz–50 MHz; the pulse width is 8 ns–999 s; the edge transition time is 5 ns–625 s; the duty cycle is 0.1–99.9%; and the pulse waveform edge time can be adjusted.



Figure 1. Arbitrary waveform generator for experiment.

2.1.2. Selection of Downhole Acoustic Transducers

As a component to convert the downhole electric energy to acoustic energy, the transducer is the core of the downhole acoustic generating device. Low-frequency longitudinal waves have become the first choice for downhole information acoustic carriers because of their fast propagation speed in drill string, small energy attenuation, and low difficulty in receiving and analyzing. Currently, the commonly used transducers for generating longitudinal waves include sandwich piezoelectric transducers and magnetostrictive transducers. However, the sandwich piezoelectric transducer is difficult to be applied downhole due to the difficulty in manufacturing, installation, and downhole power supply. The giant magnetostrictive transducer has the advantages of a large strain (5–10 times that of piezoelectric ceramics), a high output power, a high controllability, compact structure, and a wide operating temperature range (-50 – 70 °C) [29]. It is the best choice for acoustic wave generating transducers under high-temperature and high-pressure (HTHP) environments in complex and limited downhole space.

There was giant magnetostriction based on energy conversion material, using a Terfenol-D rod ($\phi 10$ mm \times 40 mm, axial strain of 1.2×10^{-3} under the pressure of 6–8 MPa, and a magnetic field strength of 10,000 kA/m). The structure of the telescopic transducer is shown in Figure 2. When the transducer is working, the pulse current generated by the power supply is applied to the excitation coil of the transducer, and the giant magnetostrictive rod produces a telescopic change under the action of the alternating magnetic field, converting the electrical energy into mechanical vibration with a certain frequency. The emission frequency is 800 Hz, and the working frequency range is 20 Hz–25 kHz.

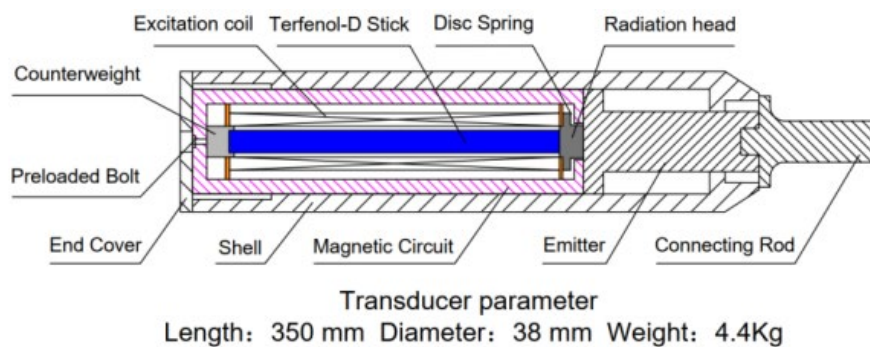


Figure 2. Structure of downhole magnetostrictive transducer.

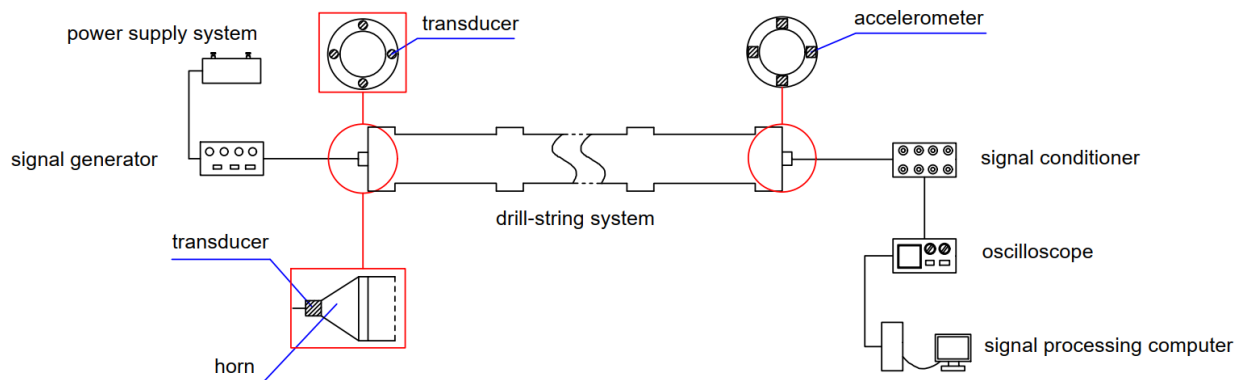
2.1.3. Optimization of Acoustic Radiation Mode in Transducer

The acoustic radiation mode refers to the way that the acoustic wave enters the drill string system from the transducer. The transducer is the core component of the downhole acoustic generator. The acoustic radiation method determines the transmission efficiency of the acoustic generator and the acoustic propagation in the drill string. Since the outlet of the giant magnetostrictive transducer is annulus, and the circular section of drill string is much larger than the transducer, the designed acoustic radiation mode of the transducer should not only ensure that the characteristics of acoustic waves are not distorted, but also that the energy loss during transmission is minimized.

The plane waves for downhole information transmission in the drill string can improve the stability and the quality of the acoustic signal. The generation of the plane wave depends on the way that radiates from the transducer into the drill string. The optimal radiation method is the outlet of the transducer which has the same annular as the drill string body, which is difficult to achieve based on giant magnetostrictive transducers in a complex and limited downhole space.

Considering the downhole installation conditions and the structural characteristics of the giant magnetostrictive transducer, two radiation modes were designed: the multi-point acoustic radiation and the single-point acoustic radiation. The circumferential multi-

point acoustic radiation is transmitting waves in the string by evenly distributed multiple transducers in the circumferential section; the horn structure is used to radiate the single point incoming acoustic signal. The transducer is installed on the small end of the horn along the axis of the string, and the acoustic wave emitted by the transducer is transmitted into the drill string through the horn for propagation. In order to select the best solution from these two modes above, two plans in Figure 3 are designed to analyze the acoustic propagation effects of different transducer acoustic radiation modes.



Scheme 2: Single point radiation through horn in circumferential direction

Figure 3. Transmission effect scheme of different acoustic radiation modes in transducer.

The acoustic signal at the receiving end under the same conditions obtained by these two tests is shown in Figure 4. It can be seen that there are obvious differences between the acoustic wave amplitudes measured by the four accelerometers that are uniformly distributed in the circumferential direction of the same receiving surface using the circumferential multi-point acoustic radiation method, indicating that the acoustic waves obtained in the drill string by this method are non-plane waves. However, there is no obvious difference in the waveform and amplitude of the received signal at different measuring points by using the single-point acoustic radiation method through horn, indicating that this method can obtain plane waves and can achieve the same propagation effect as the optimal radiation method. Therefore, the central single-point horn radiation scheme is selected as the installation form of the transducer in the downhole acoustic wave generator.

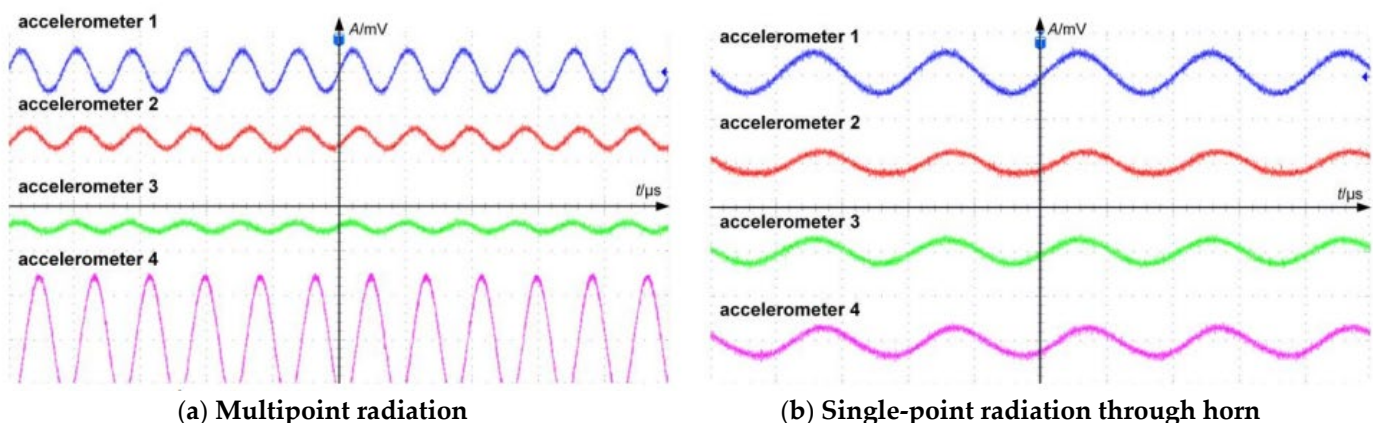


Figure 4. Transmission effect of four accelerometers under different acoustic radiation methods.

2.1.4. Signal Reception and Processing System

In order to realize the effective acquisition, real-time display, data storage, and post-processing analysis of the acoustic signal at the end of the drill string, an acoustic signal receiving and processing system is set up. The system mainly includes an acceleration sensor, signal conditioner, oscilloscope, computer, and other instruments and corresponding

data processing software. Its basic working principle is that the acceleration sensor installed on the drill string recognizes and receives the effective acoustic signal, converts the acoustic signal into the electrical signal, and transmits it to the signal conditioner through the cable. After amplifying, filtering, and screening the signal, it is transmitted to the oscilloscope and converted into a waveform image for real-time display and storage. Then, the signal is further processed and analyzed by the corresponding signal processing software.

A Lens LC0120 piezoelectric accelerometer is selected for the acceleration sensor. (range: ± 5 g; sensitivity: 1000 mV/g; frequency: 0.35 Hz–6000 Hz; installation resonance point: 18 kHz; resolution: 0.00002 g; linearity less than 1%; lateral sensitivity less than 5%; output voltage: 8–12 VDC; constant current: 2–20 mA; temperature range: -40 – 120 °C). It has the obvious advantages of a light weight, high sensitivity, and wide band. The installation method is closely connected with the drill string through magnetic adsorption. The physical installation is shown in Figure 5.

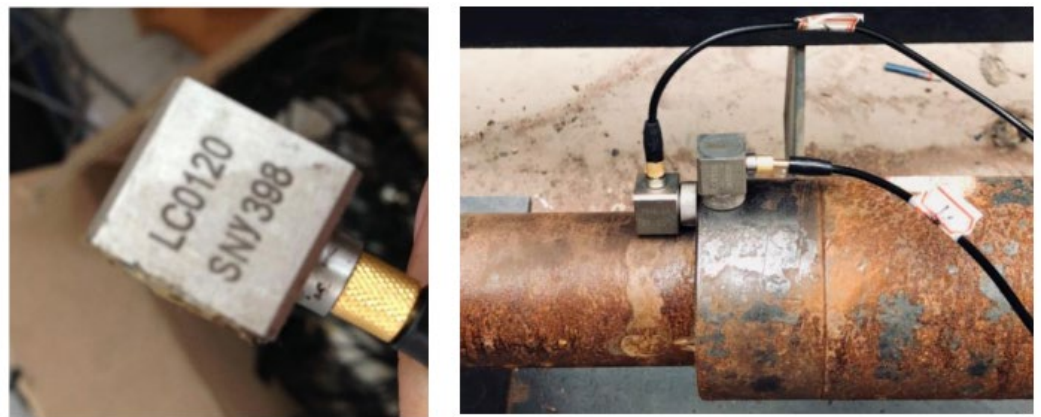


Figure 5. The acceleration transducer.

The function of the signal conditioner is to amplify, filter the signal received by the acceleration sensor, and transmit it to the oscilloscope for display. The signal conditioner used in the experiment is the Lens LC0201-5 multi-channel charge/voltage amplifier with 5 channels. In addition to the performance of a general charge amplifier, each channel can also be used in the signal processing system as a preamplifier. It has a voltage/charge input function and a voltage output function and can be connected with a voltage input sensor or a piezoelectric acceleration sensor to measure the acceleration. The constant supply current is 4 mA, the constant current supply voltage is 24 VDC, the high-frequency upper limit frequency is 30 kHz, the low-frequency lower limit frequency is 0.01 Hz, and the noise is 4 μ V with an accuracy of 0.5%. The operating temperature ranges from -10 °C to 40 °C. The connection method is shown in Figure 6.



Figure 6. Signal conditioner.

The oscilloscope selected for the experiment is Tektronix's MSO3034 series mixed-signal oscilloscope (Figure 7). It has a 100 MHz bandwidth, 4 analog channels, and 16 digital channels. Additionally, there is a sampling rate of 2.5 GS/s on every channel with a 5 M point record length. The maximum waveform capture rate is higher than 5000 wfm/s.

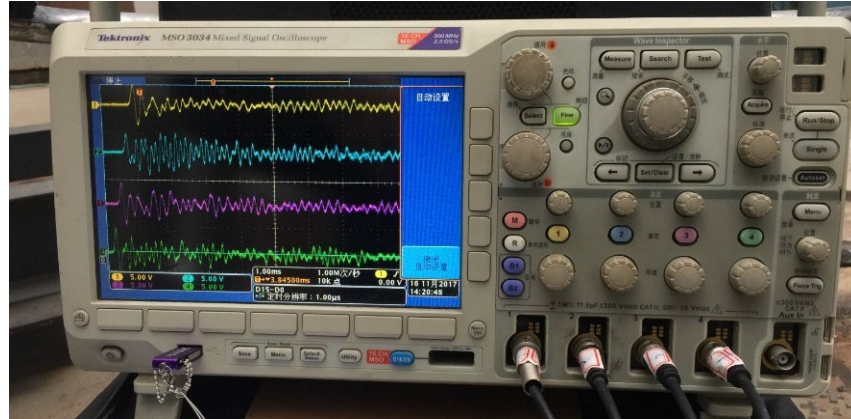


Figure 7. Oscilloscope used in the experiment.

2.2. Experiment of Acoustic Propagation in Curved Drill String

2.2.1. The Setup of the Experimental Device

In order to simulate the bending state of the drill string during the drilling process and test the acoustic propagation characteristics in the curved drill string, the setup experimental device needs to meet the following requirements: (1) the acoustic signal can be generated at one end and effectively received at the other end through the drill string, and then processed later, and (2) the bending stress in the drill string can be adjusted according to the requirements.

Based on the above requirements, the designed experimental device is shown in Figure 8, and the actual device is shown in Figure 9. The device for the acoustic propagation characteristics in a curved drill string includes four systems: an acoustic signal generation system, a simulated drill string system, a bending stress application system, and an acoustic signal receiving and processing system. The moving brackets of the bending stress application system are installed at both ends of the simulated drill string system to lift it. Then, the counterweight installation plate is installed in the middle of the drill string by adjusting the weight of the counterweight block to change the bending stress of the drill string according to the experimental requirements.

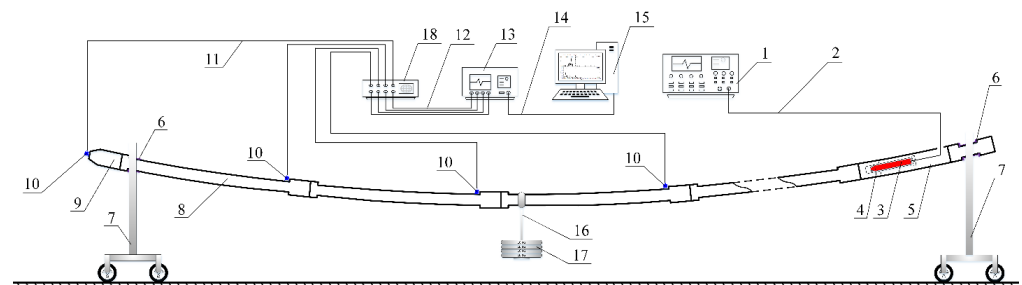


Figure 8. Experimental device. 1—arbitrary wave generator; 2—transmission circuit of acoustic generator; 3—transducer; 4—protective cover; 5—acoustic signal generating subsection; 6—sound insulation gasket; 7—moving bracket; 8—simulated drill string; 9—simplifier; 10—accelerometer; 11—transmission circuit of acoustic reception signal; 12—transmission circuit of modulated signal; 13—oscilloscope; 14—data transmission circuit; 15—signal processing system; 16—counterweight installation plate; 17—counterweight block; 18—signal conditioner.

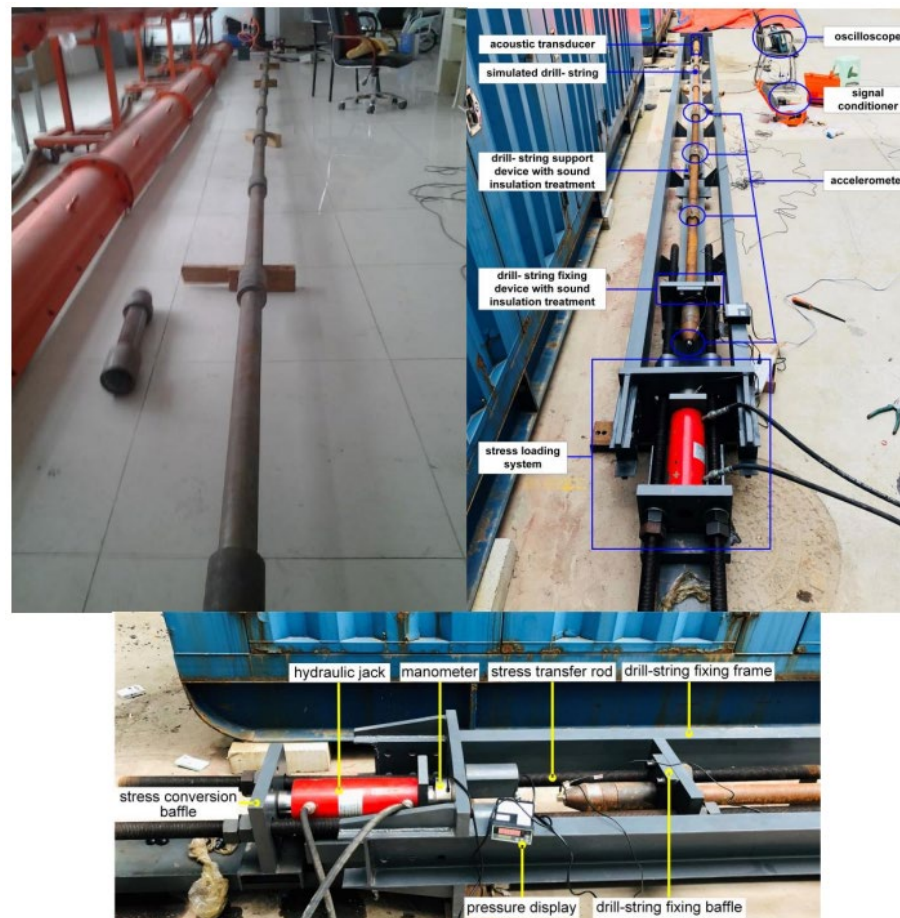


Figure 9. The actual device.

In order to ensure the reliability of the experimental results, the following acoustic insulation treatment is carried out in the experimental device. First of all, if the steel moving support is directly contacted with the drill string, it will inevitably cause energy loss. Therefore, a rubber gasket is installed at the contact position between the string and the moving support to reduce the acoustic energy loss at the contact position by using the principle of the acoustic wave impedance difference; then, the contact position between the end of the counterweight installation plate and the drill string are made of synthetic fiber materials. The difference in the column impedance is significant, so the loss of acoustic energy from this contact is also negligible.

In the experiment, the different bending states of the drill string are adjusted by the geometric principle. The bended string is equivalent to an arc in Figure 10. Due to the length of the drill string being short in the experiment, the length in different bending states remains basically unchanged. In order to quantitatively characterize the bending state of the drill string, the curvature of the drill string is defined as follows [23,30–33]:

$$\gamma = \frac{2\theta}{L} \quad (1)$$

where γ is the curvature of the drill string, $^{\circ}/10$ m; θ is the half central angle, $^{\circ}$; and L is the length of the drill string, m.

The relationship between these parameters is shown in Figure 10 according to the geometric principle, where the length L of the curved drill string is the arc length AB , which can be expressed as:

$$\widehat{AB} = \frac{\pi R\theta}{90} \quad (2)$$

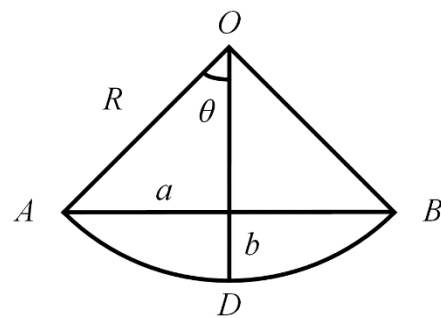


Figure 10. Equivalent geometric model of curved drill string.

The relationship between a , b and R , θ can be calculated from the geometric relationship:

$$\begin{aligned} a &= R \cdot \sin \theta \\ b &= R \cdot (1 - \cos \theta) \end{aligned} \quad (3)$$

The length of the simulated drill string used in the experiment is 10 m, and the corresponding parameters are shown in Table 1. During the experiment, the bending stress in the drill string is changed by adjusting the weight of the counterweight in the middle of the drill string to change the bending state. According to this principle, the value b is adjusted by changing the weight of the counterweight in the middle of the drill string since the height of the bracket is fixed, and then the quantified curvature of the drill string can be obtained by the value b .

Table 1. Adjustment parameter of drill string curvature.

$\theta/^\circ$	R/m	a/m	b/m	Curvature $\gamma/(^\circ/10 \text{ m})$
1	286.48	4.999	0.050	2
2	143.24	4.999	0.090	4
3	95.50	4.998	0.131	6
4	71.62	4.996	0.174	8
5	57.30	4.994	0.218	10

2.2.2. Experimental Process

In order to study the effect of different pulse repetition rates, excitation voltages, and pulse widths on the acoustic propagation characteristics in the curved drill string, the setup experimental device was used to analyze the acoustic propagation characteristics under different working conditions. The specific experimental scheme is shown in Table 2. The experimental process is shown as follows:

- (1) Ten simulated drill string with a length of 1.0 m were selected and connected as acoustic wave transmission channels;
- (2) One end of the drill string was connected with an acoustic signal generating sub of a magnetostrictive transducer through a screw thread, and a triaxial acceleration sensor for receiving acoustic signals was installed at the axial position of the end of the drill string;
- (3) The simulated drill string was installed on the moving bracket, the bracket was fixed near the receiving end, and the counterweight mounting plate was installed in the middle of the drill string;
- (4) The low-frequency pulse signal was applied by the transducer, the pulse repetition rate was adjusted to 5 Hz, the excitation voltage was 100 V, and the pulse width was 5 μs ;
- (5) The bending state of the drill string was adjusted by the counterweight in the counterweight installation plate and the experiment was repeated in the curvature of $0^\circ/10 \text{ m}$, $2^\circ/10 \text{ m}$, $6^\circ/10 \text{ m}$, and $10^\circ/10 \text{ m}$, respectively;

- (6) The pulse repetition rate was replaced by 1 Hz and 10 Hz, keeping other experimental conditions unchanged, and then step (5) was repeated;
- (7) The excitation voltage was replaced by 300 V, keeping other experimental conditions unchanged, and then step (5) was repeated;
- (8) The pulse width was replaced by 1000 μs and 10,000 μs , keeping other experimental conditions unchanged, and then step (5) was repeated;
- (9) Fourier transform was performed on the received signals to obtain the acoustic spectrum under different experimental conditions.

Table 2. Experimental scheme of acoustic propagation characteristics in curved drill string.

Scheme Number	Pulse Repetition Rate/Hz	Excitation Voltage/V	Pulse Width/ μs	Curvature γ /($^{\circ}$ /10 m)
1				0
2				2
3	1	100	5	4
4				6
5				0
6				2
7	5	100	5	4
8				6
9				0
10				2
11	10	100	5	4
12				6
13				0
14				2
15	5	300	5	4
16				6
17				0
18				2
19	5	100	1000	4
20				6
21				0
22				2
23	5	100	10,000	4
24				6

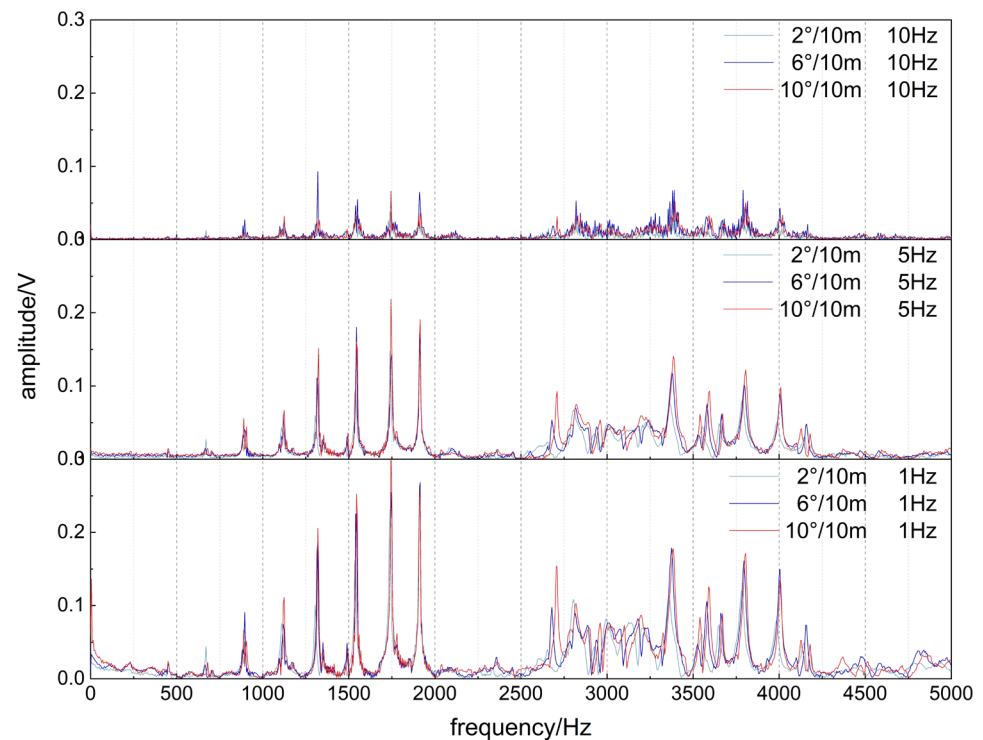
3. Results

3.1. Pulse Repetition Rate

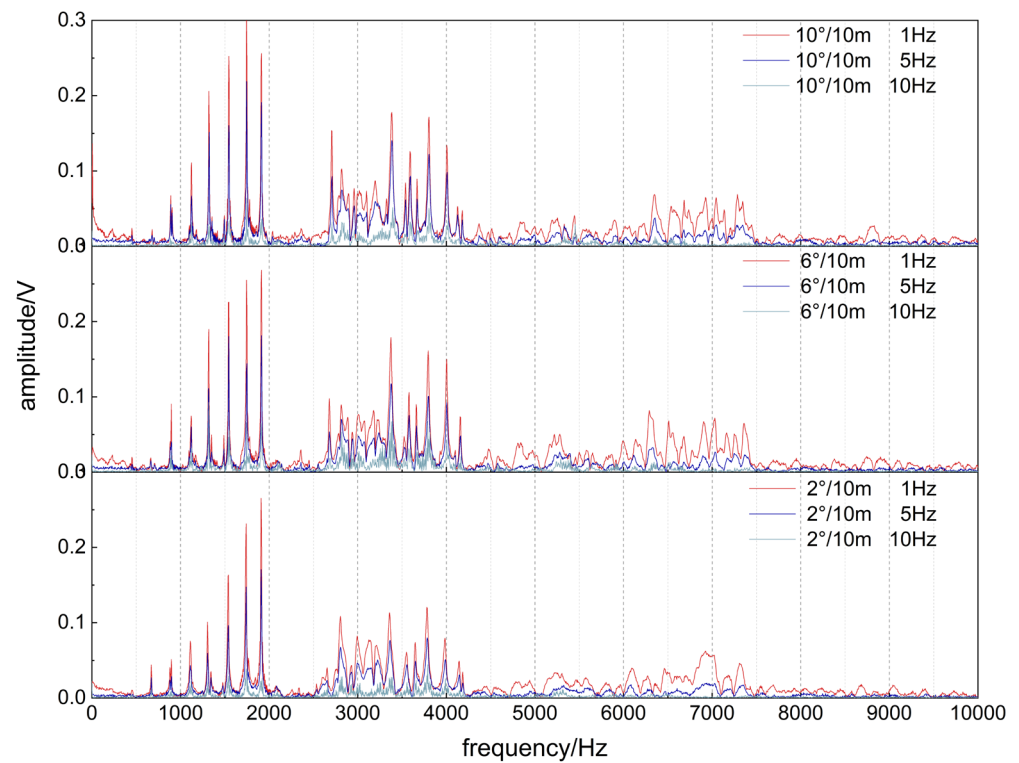
The acoustic spectrum of the curved drill string (1#–4#, 5#–8#, 9#–12#) under different pulse repetition rates was compared, and the influence of the pulse repetition rate on the acoustic propagation characteristics under different curvatures was analyzed. Figure 11 shows the spectral comparison of drill strings with different curvatures under different pulse repetition rates. It can be seen from Figure 11a that the basic structure of the frequency band remains unchanged with the increase in the curvature. The pass/stop bands are alternately distributed, and the attenuation degree of a high frequency is higher than that of a low frequency.

The passbands at different pulse repetition rates are concentrated in the 0–7500 Hz, and the passbands with higher amplitudes are concentrated in the 0–4200 Hz. In addition, the influence rule of the passband amplitude under different pulse repetition rates are different. When the repetition rate is 1 Hz, the passband amplitude in the 0–4200 Hz band increases gradually, and the passband amplitude in the 4200 Hz–7500 Hz band increases then decreases; when the repetition rate is 5 Hz, the passband amplitude increases gradually, and when the repetition rate is 10 Hz, the passband amplitude increases then

decreases. The main passband positions in the range of 0–4500 Hz are slightly shifted to a high frequency, and the high frequency offset is larger than the low frequency.



(a)



(b)

Figure 11. Comparison of acoustic spectrum under different pulse repetition rates and curvatures. (a) Curvature comparison; (b) comparison of pulse repetition rate.

Figure 11b shows the spectral comparison at the same curvature at different pulse repetition rates. It can be seen from Figure 11b that the effect of the pulse repetition rate on the acoustic propagation characteristics under different curvatures is similar. The pass/stop bands are alternately distributed with the increase in the pulse repetition rate, and the attenuation degree of a high frequency is greater than that of low frequency. In addition, the passbands at different pulse repetition rates are concentrated in the 0–7500 Hz frequency band, and the passbands with larger amplitudes are concentrated in the 0–4200 Hz frequency band. The passband amplitude gradually decreased with an increasing pulse repetition rate, and the passband amplitude at 1 Hz/5 Hz was significantly higher than that at 10 Hz.

From the above analysis, it can be seen that the curvature of the drill string under different pulse repetition rates mainly affects the passband amplitude, and the effect on the passband position is significantly smaller than that on the passband amplitude and the passband width. In order to further compare the effect differences of the string curvature and pulse repetition rate on the passband amplitude, the continuous integration of the spectrum on the x-axis is shown in Figure 12. It can be seen from Figure 12 that the influence of the pulse repetition rate on the passband amplitude is significantly higher than that of the curvature. The amplitude of the passband gradually decreases with the increase in the pulse repetition rate under the same curvature; the amplitude of the passband gradually increases with the increase in the curvature under the same pulse repetition rate.

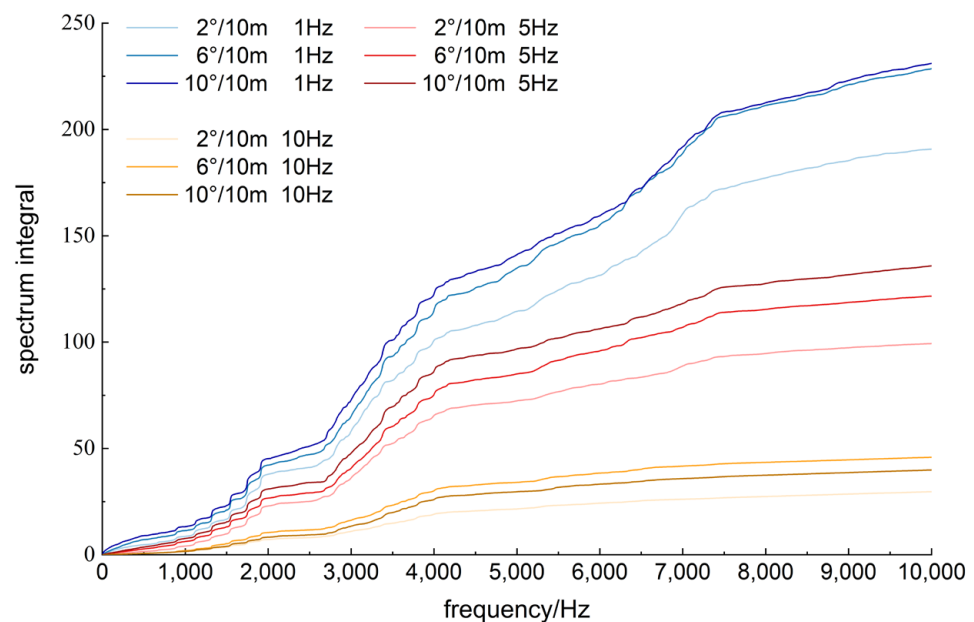


Figure 12. Comparison of spectral integrals under different pulse repetition rates and curvatures.

3.2. Excitation Voltage

The acoustic spectrum of the curved drill string (5#–8#, 13#–16#) under different excitation voltages was compared, and the influence of the excitation voltage on the acoustic propagation characteristics under different curvatures was analyzed. Figure 13 shows the spectral comparison in drill strings with different curvatures under two different excitation voltages. It can be seen from Figure 13a that the basic structure of the frequency band remains unchanged with the increase in the string curvature. The pass/stop bands are alternately distributed, and the attenuation degree of a high frequency is higher than that of a low frequency.

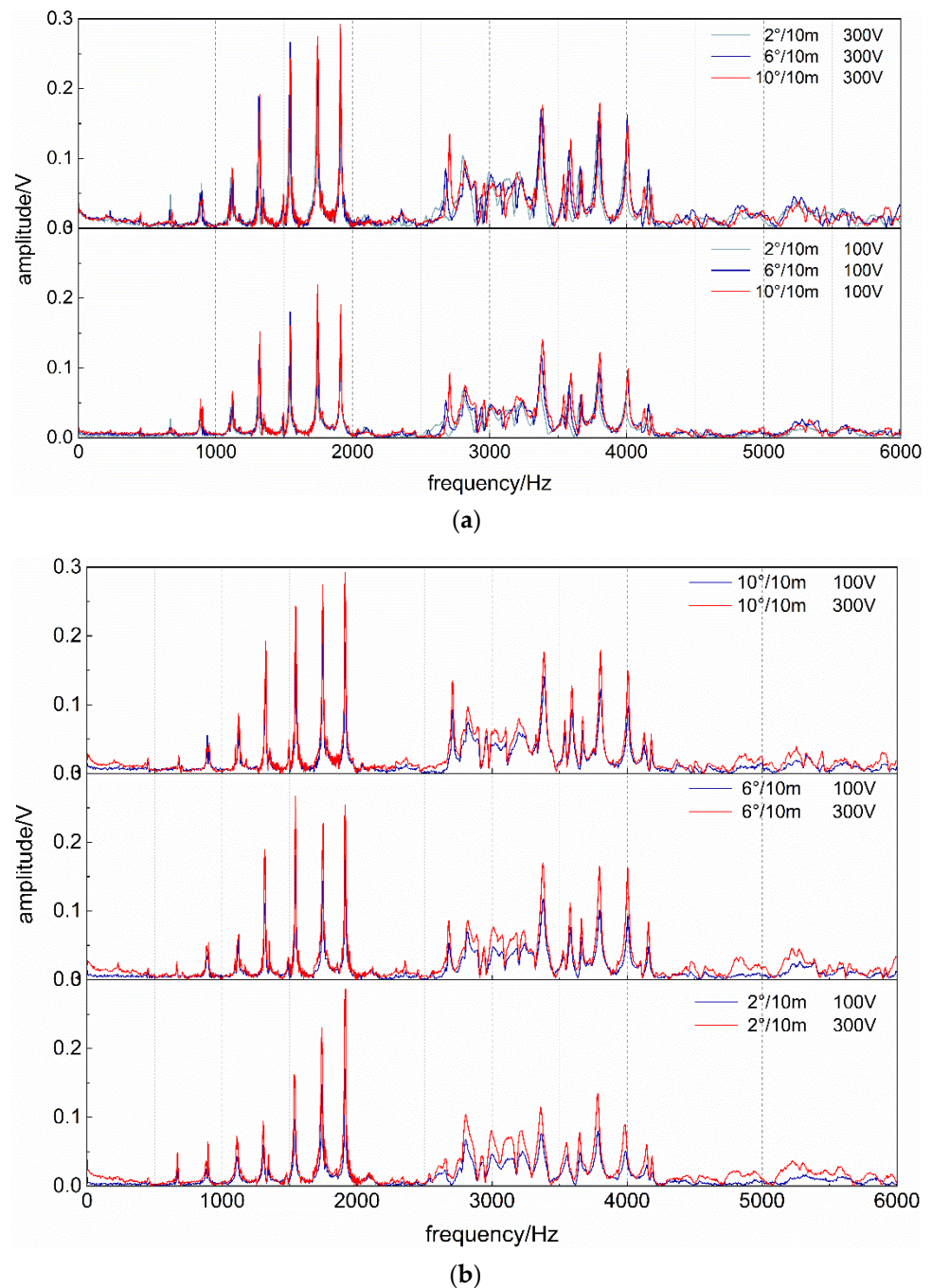


Figure 13. Comparison of acoustic spectrum with different excitation voltage and curvatures. (a) Curvature comparison; (b) comparison of excitation voltage.

The passbands at different pulse repetition rates are concentrated in the 0–7500 Hz range, and the passbands with larger amplitudes are concentrated in the 0–4200 Hz range. In addition, the influence rule of the passband amplitude under different excitation voltages is basically the same: the passband amplitude increases gradually in the 0–4200 Hz frequency band, and the passband amplitude changes irregularly in the 4200–7500 Hz frequency band. The main passband positions in the range of 0–4500 Hz are slightly shifted to the high frequency under different excitation voltages, and the high-frequency offset is higher than the low frequency.

Figure 13b shows the spectrum comparison under different excitation voltages and the curvatures. It can be seen from Figure 13b that the excitation voltage has a similar

effect on the acoustic propagation characteristics under different curvatures. The basic structure of the frequency band remains unchanged with the increase in the excitation voltage, the pass/stop bands are alternately distributed, and the attenuation degree of a high frequency is higher than that of a low frequency. In addition, the passbands at different pulse repetition rates are concentrated in the 0–7500 Hz frequency band, and the passbands with higher amplitudes are concentrated in the 0–4200 Hz frequency band. The amplitude of the passband increases gradually with the increase in the excitation voltage, and the width and position of the passband remain unchanged.

From the above analysis, it can be seen that the curvature of the drill string under different excitation voltages mainly affects the passband amplitude and the effect on the passband position is significantly smaller than that on the passband amplitude and the passband width. In order to further compare the effect differences of the curvature and excitation voltage on the passband amplitude, the continuous integration of the spectrum on the x-axis is shown in Figure 14. It can be seen from Figure 14 that the influence of the excitation voltage on the passband amplitude is significantly higher than that of the curvature. The amplitude of the passband increases with the increase in the excitation voltage under the same curvature; the amplitude of the passband increases gradually with the increase in the curvature under the same excitation voltage.

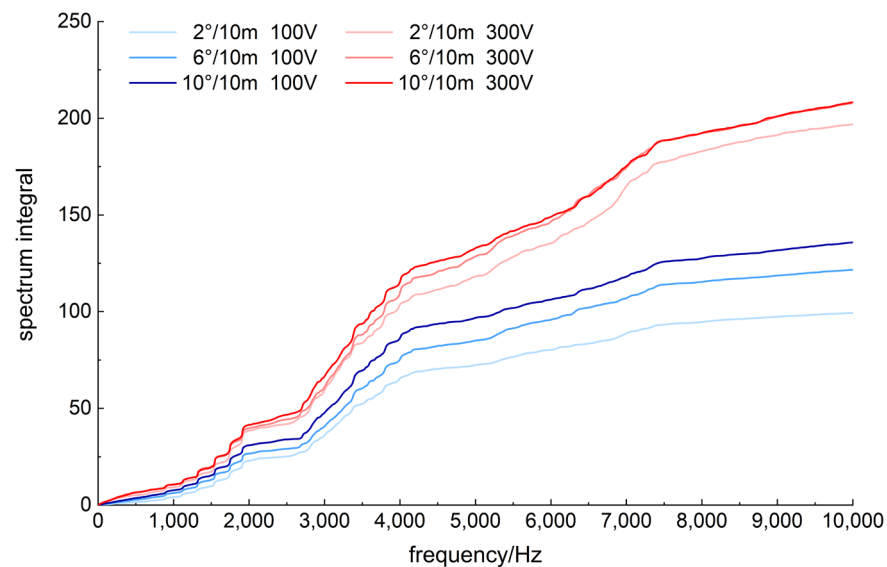
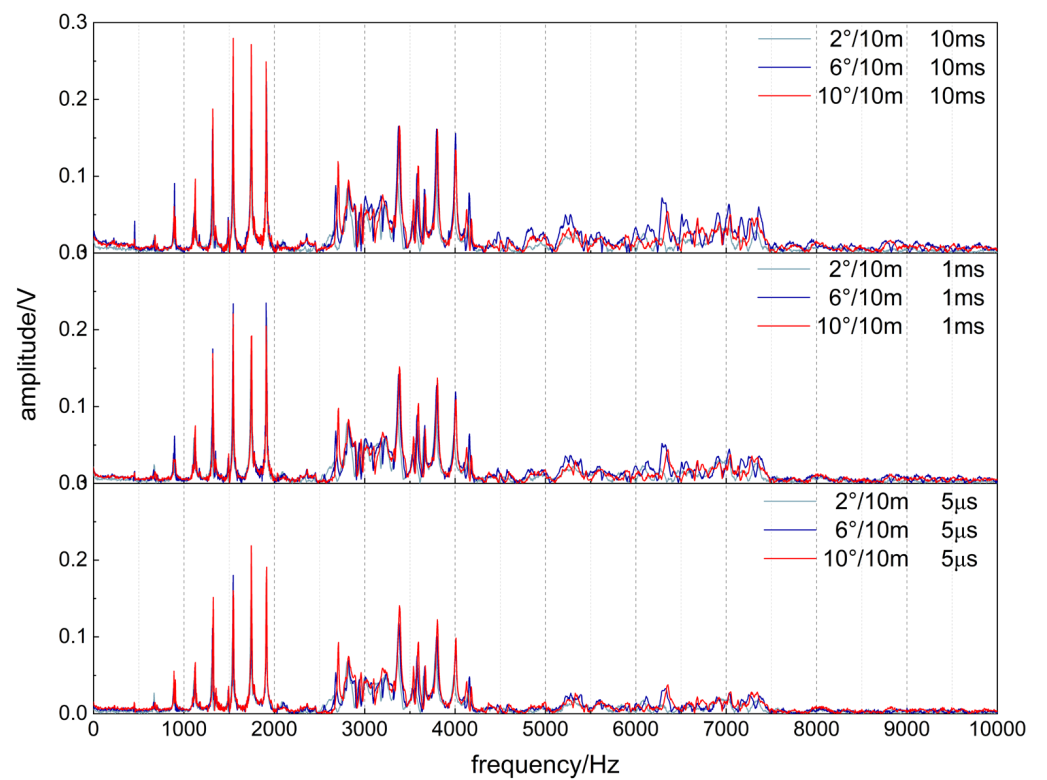


Figure 14. Comparison of spectral integrals under different excitation voltages and curvatures.

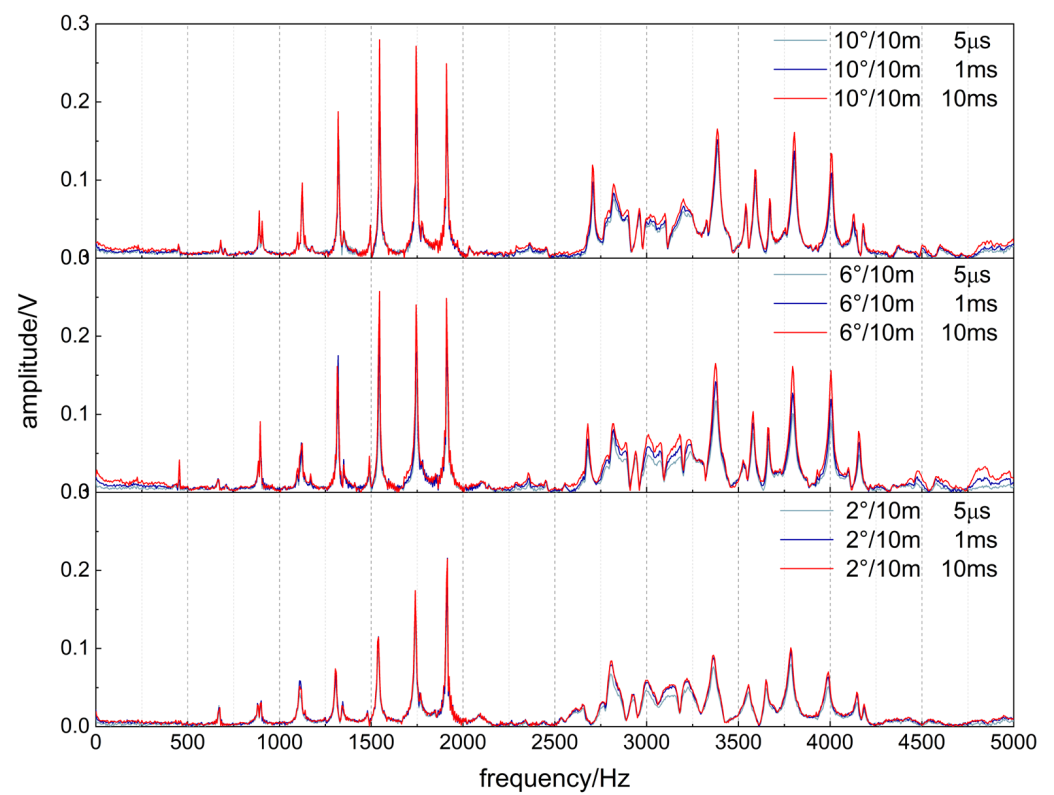
3.3. Pulse Width

The acoustic spectrum of the curved drill string with different pulse widths (5#–8#, 17#–20#, 20#–24#) was compared, and the influence of the pulse width on the acoustic propagation characteristics under different curvatures was analyzed. Figure 15 shows the spectral comparison of drill strings with different curvatures under different pulse widths. It can be seen from Figure 15a that the basic structure of the frequency band remains unchanged with the increase in the curvature, the pass/stop bands are alternately distributed, and the attenuation degree of a high frequency is higher than that of a low frequency.

The passbands at different pulse repetition rates are concentrated in the 0–7500 Hz range, and the passbands with higher amplitudes are concentrated in the 0–4200 Hz range. In addition, the influence rule of the passband amplitude under different pulse widths is basically the same: the passband amplitude in the 0–4200 Hz band increases gradually, and the passband amplitude in the 4200–7500 Hz band first increases and then decreases. The main passband positions in the range of 0–4500 Hz are slightly shifted to a high frequency under different pulse widths, and the high-frequency offset is higher than the low frequency.



(a)



(b)

Figure 15. Comparison of acoustic spectrum with different pulse widths and different curvatures. (a) Curvature comparison; (b) comparison of pulse width.

Figure 15b shows the spectral comparison of the same curvature with different pulse widths. It can be seen from Figure 15b that the pulse width has a similar effect on the acoustic propagation characteristics under different curvatures. The basic structure of the frequency band remains unchanged as the pulse width increases, the pass/stop bands are alternately distributed, and the attenuation degree of a high frequency is higher than that of a low frequency. The passbands with different pulse widths are concentrated in the 0–7500 Hz frequency band, and the passbands with larger amplitudes are concentrated in the 0–4200 Hz frequency band. The passband amplitude increases gradually with the increase in the pulse width, and the passband width and position remain unchanged.

From the above analysis, it can be seen that the curvature of the drill string under different pulse widths mainly affects the passband amplitude, and the influence degree on the passband position is significantly smaller than that on the passband amplitude and the passband width. In order to further compare the effect differences in the curvature and pulse width on the passband amplitude, the continuous integration of the spectrum on the x-axis are shown in Figure 16. It can be seen from Figure 16 that the influence of the pulse width on the passband amplitude is significantly higher than that of the curvature. The amplitude of the passband increases with the increase in the pulse width under the same curvature; the amplitude of the passband increases first and then decreases with the increase in the curvature under the same pulse width.

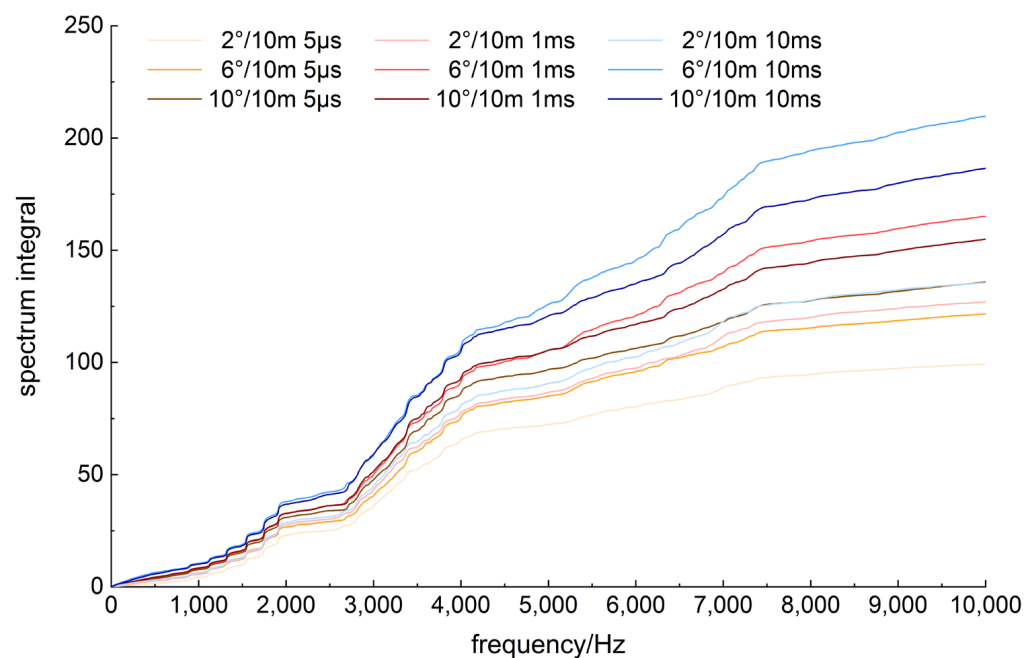


Figure 16. Comparison of spectral integrals under different pulse widths and curvatures.

4. Discussion

The propagation characteristics of acoustic waves with different pulse repetition rates, excitation voltages, and pulse widths in a curved drill string are tested by an experimental device in this paper. The curvature of the drill string does not change the basic structure of the acoustic band, but it does have a slight influence on the amplitude and the passband position. The degree of influence on the amplitude is higher than that on the position of the passband. As the curvature increases, the amplitude gradually increases and the passband gradually shifts to the high frequency. The high-frequency migration is larger than the low frequency.

(1) The bending of the drill string does not change the basic structure of the acoustic frequency band and it has no obvious effect on the acoustic propagation characteristics. It has a slight influence on the passband amplitude and the passband position, and the passband has a great influence on the amplitude and the influence on the passband position.

The bending degree increases and the amplitude increases gradually. (2) As the bending degree increases, the passband gradually shifts to a high frequency, and the high-frequency shift is greater than the low frequency, which verifies the correctness of the theoretical analysis. (3) The pulse repetition rate, excitation voltage, and pulse width only affect the passband amplitude, and the influence degree is significantly greater than that of the drill string bending. With the increase in the pulse repetition rate, the amplitude of the passband decreases gradually, and with the increase in the excitation voltage and pulse width, the amplitude of the passband increases gradually.

Based on that, the basic characteristics of the acoustic signal passing through the curved drill string do not change when applying the acoustic wave transmission technology in horizontal wells, but the attenuation characteristics and the position of the passband are changed, and the degree of the attenuation characteristics is higher than that of the passband position. Therefore, the influence of the curvature on the acoustic propagation characteristics can be reduced or avoided by optimizing the acoustic excitation parameters, increasing the distance between the adjacent repeaters and avoiding the interference frequency band as the carrier frequency band, so as to ensure that the acoustic wave signal is transmitted in the curved drill string stably.

5. Conclusions

- (1) An experimental device for acoustic propagation characteristics in a curved drill string was set up, and the device was used to test the acoustic propagation characteristics in drill strings under different pulse repetition rates, excitation voltages, and pulse widths. The curvature has an impact on the acoustic propagation in the drill string; there are still alternately arranged pass/stop bands when the acoustic wave propagates. The passband has a more significant effect on the amplitude than the position.
- (2) As the curvature of the drill string increases, the amplitude of the passband increases and the passband moves backward. The higher the frequency, the higher the amplitude backward shift. The pulse repetition rate, excitation voltage, and pulse width only affect the passband amplitude.
- (3) The low-frequency passband is less affected by the curved drill string in directional wells. After considering the influence of the curvature on the acoustic transmission, the low-frequency signal should be preferentially selected as the carrier for the acoustic transmission of the downhole information.

Author Contributions: Conceptualization, Q.W. and H.W.; methodology, C.B.; validation, J.Z.; supervision, Z.G.; project administration, J.Z. All authors have read and agreed to the published version of the manuscript.

Funding: This paper was research was funded by Project funded by China Postdoctoral Science Foundation (No. 2021M693508), Basic research and strategic reserve technology research fund project of institutes directly under CNPC (No. 2021DQ03-17), China National Natural Foundation (No. 51574275 & 51404285), CNPC Key core technology research projects (No. 2022ZG06).

Data Availability Statement: Not applicable.

Acknowledgments: The authors would like to acknowledge the academic and technical support of CNPC.

Conflicts of Interest: The authors declare that they have no known competing financial interest or personal relationship that could have appeared to influence the work reported in this paper.

References

1. Barnes, T.G.; Kirkwood, B.R. Passbands for acoustic transmission in an idealized drill string. *J. Acoust. Soc. Am.* **1972**, *5*, 1606–1608. [[CrossRef](#)]
2. Berro, M.J.; Reich, M. Laboratory investigations of a hybrid mud pulse telemetry (HMPT)—A new approach for speeding up the transmitting of MWD/LWD data in deep boreholes. *J. Pet. Sci. Eng.* **2019**, *183*, 106374. [[CrossRef](#)]
3. Cai, W. An experimental study on the propagation characteristics of acoustic waves in drill strings. *Nat. Gas Ind.* **2016**, *36*, 72–77.
4. Chaumillon, R.; Romeas, T.; Paillard, C.; Bernardin, D.; Giraudet, G.; Bouchard, J.F.; Faubert, J. Enhance data visualization to capture the simulator sickness phenomenon: On the usefulness of radar charts. *Data Brief* **2017**, *13*, 301–305. [[CrossRef](#)]
5. Drumheller, D.S. Acoustical properties of drill strings. *J. Acoust. Soc. Am.* **1989**, *85*, 1048–1064. [[CrossRef](#)]
6. Guan, Z.; Liu, Y.; Zhao, G.; Wang, W. Influence of the drill-string structure diversity on acoustic transmission characteristics. *Acta Pet. Sin.* **2012**, *33*, 687–691.
7. Jia, D.; Cui, C.; Wang, S. Propagation properties of acoustic waves inside periodic pipelines. *Inf. Sci.* **2014**, *275*, 360–369. [[CrossRef](#)]
8. Li, C.; Ding, T. Effect of damping boundary conditions on acoustic transmission of drill strings. *J. Vib. Shock* **2006**, *25*, 17–20.
9. Li, C.; Ding, T. Influence of discontinuous boundaries on acoustic transmission in periodic cascade with application to drill pipes. *J. Vib. Shock* **2006**, *25*, 172–175.
10. Li, Z.; Elsworth, D. Controls of CO₂-N₂ gas flood ratios on enhanced shale gas recovery and ultimate CO₂ sequestration. *J. Pet. Sci. Eng.* **2019**, *179*, 1037–1045. [[CrossRef](#)]
11. Li, Z.; Yin, J.; Zhu, D.; Akhil, D.G. Using downhole temperature measurement to assist reservoir characterization and optimization. *J. Pet. Sci. Eng.* **2011**, *78*, 454–463. [[CrossRef](#)]
12. Liu, H.; Liu, A.; Zhang, B. A fuzzy comprehensive evaluation method of maintenance quality based on improved radar chart. In Proceedings of the ISECS International Colloquium on Computing Communication, Control and Management, Guangzhou, China, 3–4 August 2008; pp. 638–642.
13. Liu, Y.; Guan, Z.; Zhao, G. Text for acoustic propagation characteristics in drill string composed of size-difference drill pipes. *J. Vib. Shock* **2015**, *34*, 93–97.
14. Lu, N.; Hou, J.; Liu, Y.; Barrufet, M.A.; Ji, Y.; Xia, Z.; Xu, B. Stage analysis and production evaluation for class III gas hydrate deposit by depressurization. *Energy* **2018**, *165*, 501–511. [[CrossRef](#)]
15. Ma, D.; Shi, Y.; Zhang, W.; Liu, G. Design of acoustic transmission along drill strings for logging while drilling data based on adaptive NC-OFDM. *AEU-Int. J. Electron. Commun.* **2018**, *83*, 329–338. [[CrossRef](#)]
16. Qiao, P.; Wu, Z.; Li, H. Power quality synthetic evaluation based on improved radar chart. *Electr. Power Autom. Equip.* **2011**, *31*, 88–92.
17. Shao, J.; Yan, Z.; Han, S.; Li, H.; Gao, T.; Hu, X.; Wei, C. Differential signal extraction for continuous wave mud pulse telemetry. *J. Pet. Sci. Eng.* **2017**, *148*, 127–130. [[CrossRef](#)]
18. Su, Y. Introduction to the theory and technology on downhole control engineering and its research progress. *Pet. Explor. Dev.* **2018**, *45*, 754–763. [[CrossRef](#)]
19. Sun, Y.; Zhang, F.; Wang, Q.; Gao, K. Application of “Crust 1” 10k ultra-deep scientific drilling rig in Songliao basin drilling project (CCSD-SKII). *J. Pet. Sci. Eng.* **2016**, *145*, 222–229. [[CrossRef](#)]
20. Wang, Y.; Li, Y. Comprehensive evaluation of power transmission and transformation project based on improved radar chart. *Adv. Mater. Res.* **2011**, *354–355*, 1068–1072. [[CrossRef](#)]
21. Zheng, L.; Yu, J.; Yang, Q.; Gao, Y.; Sun, F. Vibration wave downhole communication technique. *Pet. Explor.* **2017**, *44*, 321–327. [[CrossRef](#)]
22. Gao, L.; Gardner, W.R.; Robbins, C.; Memarzadeh, M.; Johnson, D. Limits on data communication along the drill string using acoustic waves. *SPE Reserv. Eval. Eng.* **2008**, *11*, 141–146. [[CrossRef](#)]
23. Su, Y.D.; Tang, X.M.; Xu, S.; Zhuang, C.X. Acoustic isolation of a monopole logging while drilling tool by combining natural stopbands of pipe extensional waves. *Geophys. J. Int.* **2015**, *202*, 439–445. [[CrossRef](#)]
24. Zeng, S.; Li, D.; Wilton, D.R.; Chen, J. Fast and accurate simulation of electromagnetic telemetry in deviated and horizontal drilling. *J. Pet. Sci. Eng.* **2018**, *166*, 242–248. [[CrossRef](#)]
25. De, G.P.; Grudzinski, R. Propagation of electromagnetic waves along a drill string of finite conductivity. *SPE Drill. Eng.* **1987**, *2*, 127–134.
26. Drumheller, D.S. Wave impedances of drill strings and other periodic media. *J. Acoust. Soc. Am.* **2002**, *112*, 2527–2539. [[CrossRef](#)] [[PubMed](#)]
27. Wang, Q.; Guan, Z.C.; Zhang, B.; Liu, Y.; Li, C. Multilevel method based on improved radar chart to evaluate acoustic frequency spectrum in periodic pipe structure. *J. Pet. Sci. Eng.* **2020**, *189*, 106878. [[CrossRef](#)]
28. Wang, Q.; Guan, Z.C.; Liu, Y.W. Acoustic frequency spectrum characteristics in periodic drill string under tension. *Energy Sci. Eng.* **2020**, *8*, 2747–2759. [[CrossRef](#)]
29. Zhao, J.; Li, J.; Cao, Q.; Bai, Y.; Wu, W.; Ma, Y. Quasi-continuous hydrocarbon accumulation: An alternative model for the formation of large tight oil and gas accumulations. *J. Pet. Sci. Eng.* **2019**, *174*, 25–39. [[CrossRef](#)]
30. Hui, Z.; Zhang, C.; Wang, Y.; Wen, C.; Sladek, J.; Sladek, V. A local RBF collocation method for band structure computations of 2D solid/fluid and fluid/solid phononic crystals. *Int. J. Numer. Methods Eng.* **2017**, *110*, 467–500.

31. Hui, Z.; Zhang, C.; Wang, Y.; Sladek, J.; Sladek, V. A meshfree local RBF collocation method for anti-plane transverse elastic wave propagation analysis in 2D phononic crystals. *J. Comput. Phys.* **2016**, *305*, 997–1014.
32. Cao, L.; Sun, J.; Zhang, B.; Lu, N.; Xu, Y. Sensitivity analysis of the temperature profile changing law in the production string of a high-pressure high-temperature gas well considering the coupling relation among the gas flow friction, gas properties, temperature, and pressure. *Front. Phys.* **2022**, *10*, 1050229. [[CrossRef](#)]
33. Zhang, B.; Lu, N.; Guo, Y.; Wang, Q.; Cai, M.; Lou, E. Modeling and analysis of sustained annular pressure and gas accumulation caused by tubing integrity failure in the production process of deep natural gas wells. *J. Energy Resour. Technol.* **2022**, *144*, 063005. [[CrossRef](#)]

Disclaimer/Publisher's Note: The statements, opinions and data contained in all publications are solely those of the individual author(s) and contributor(s) and not of MDPI and/or the editor(s). MDPI and/or the editor(s) disclaim responsibility for any injury to people or property resulting from any ideas, methods, instructions or products referred to in the content.